Sources of Atmospheric Fine Particles and Mercury in New Jersey

Alexander Polissar, Ph.D.,
Division of Science and Research, NJDEP

September 2023

State of New Jersey
Phil Murphy, Governor

Department of Environmental Protection
Shawn M. LaTourette, Commissioner

Division of Science & Research
Nicholas A. Procopio, Ph.D., Director

Visit the DSR website:
https://dep.nj.gov/dsr

ABSTRACT

Statistical analyses showed that the annual mercury wet deposition levels in New Jersey did not decline substantially despite new regulations that significantly reduced mercury emissions in New Jersey. To explain this and to identify possible sources of air pollution in New Jersey, a receptor modeling study was conducted. The goal of the study was identification of the major sources of fine particles ($PM_{2.5}$) and mercury (Hg) in New Jersey and investigation of changes in their contributions over time. An advanced factor analysis method, Positive Matrix Factorization (PMF), was used as a receptor modeling tool for the combined mercury and chemical composition particulate data set from Brigantine, New Jersey. Different sources of air pollution, such as coal and oil combustion, metal production, wood combustion, soil, and sea salt emissions, have been identified. Midwestern coal combustion was identified as a major source for $PM_{2.5}$ in New Jersey. Time series for the three sources – oil combustion source with high loadings of V and Ni, coal combustion source with high loadings of $SO_4^{=}$, and incineration/metal production source with high loadings of Pb and Zn showed a negative trend. Major sources of the different mercury fractions have been identified as well. Time series for some of these sources, related to mercury emissions, showed a negative trend, while others exhibited no trend. Further research is necessary to determine the reasons behind the lack of decline in wet deposition of mercury. The results of the receptor modeling show that the PMF represents a useful and important tool for identifying and quantifying the sources of air pollutants.

Please cite as: Polissar, Alexander. 2023. Sources of Atmospheric Fine Particles and Mercury in New Jersey. New Jersey Department of Environmental Protection. Trenton, NJ. 32 pages. Available at https://dspace.njstatelib.org/handle/10929/112000.

INTRODUCTION

Fine aerosol particles less than 2.5 μm in diameter ($PM_{2.5}$) in the ambient air are typically composed of complex mixtures of chemical compounds, originating from a wide range of natural sources and human activities. They are often transported over long distances from their origins. The presence of anthropogenic aerosol in the atmosphere may result in changes in the solar radiation balance and visibility plus cause long-term damage to human and environmental health. For these reasons, the investigation of the spatial and temporal variations of the aerosol concentration, long-range transport, and the identification of possible sources of the aerosol are important. The results of the investigation could be useful for the understanding of mechanisms of transport and transformation of the atmospheric aerosol and improvement of the emission control strategies.

The U.S. EPA regulatory programs for the fine particles ($PM_{2.5}$) and regional haze have led to a dramatic expansion of ambient measurements of $PM_{2.5}$ mass and its chemical composition. Vast amounts of complex new data became available for developing efficient emissions control strategies to attain national health-based air quality standards. Receptor models, which attribute pollution to sources through statistical and/or meteorological interpretation of ambient measurement data, proved to be useful $PM_{2.5}$ air quality management and research tools, especially as the quantity and quality of speciated fine particle data increases and as improved methods are developed (Hopke, 1991; Kim and Hopke, 2004). Positive matrix factorization (PMF) (Paatero and Tapper, 1994) is the state-of-the-art multivariate statistical model that has potential applicability to analysis of speciated fine particle data.

It was found that most of the aerosols in the Northeastern US have similar composition profiles and seasonal variations (Song et al., 2001). About 80% of the fine particulate mass in Vermont was from secondary aerosol production, fuel combustion, wood smoke, and municipal waste incineration (Polissar et al., 2001). More than 60% of the fine mass in Vermont was from the Midwestern US sources (Polissar et al., 2001). Similar results for New Jersey were obtained (Lee et al., 2001; Kim and Hopke, 2004). Eleven sources were identified: sulfate-rich secondary aerosol I, gasoline vehicle emissions, aged sea salt, sulfate-rich secondary aerosol II, nitrate-rich secondary aerosol, sulfate-rich secondary aerosol III, sea salt emissions, airborne soil, diesel exhaust emission, incinerator, and oil combustions emissions (Kim and Hopke, 2004). Temperature-resolved carbon fractions improved source separations including three sulfate-rich secondary aerosols and two traffic-related sources that had different abundances of carbon fractions different between sources (Kim and Hopke, 2004).

Mercury emitted into the air can be transported over long distances in the atmosphere before it is eventually deposited. Exposure to mercury has a negative impact on human health. Mercury pollution is also harmful for wildlife and ecosystems. It was shown that mercury wet deposition levels and fish tissue concentrations in New Jersey did not decline despite new regulations that significantly reduced mercury emissions in New Jersey (Fig. 1) (Buchanan et al., 2023). It was found that of the 19 Mercury Deposition Network national sites with data records from 1997–2013, 10 had significant negative trends in Hg concentration in wet deposition (Weiss et al., 2016). The trend in gaseous elemental Hg from short-term datasets merged as one continuous record (81 sites) was broadly consistent with trends in Hg concentration in wet deposition, with the early time period (1998–2007) producing a significantly negative trend ($-1.5 \pm 0.2\%$ year^{-1}) and the recent time period (2008–2013) displaying a flat slope ($-0.3 \pm 0.1\%$ year^{-1}, not significant).The observed shift was explained by the effects of rising Hg emissions from regions outside the U.S. (Weiss et al., 2016).

To identify the sources of air pollution, including mercury, this receptor modeling study was conducted. An advanced factor analysis method, Positive Matrix Factorization (PMF), was used as a statistical tool for the combined mercury and chemical composition particulate data set from Brigantine, New Jersey.

OBJECTIVES

The receptor modeling study had the following objectives:

- Perform a statistical analysis of the $PM_{2.5}$ and mercury data from Brigantine, NJ,
- Determine the sources of the fine particles and mercury via PMF,
- Investigate of the long-term trends and seasonal variability in the PMF results from Brigantine, NJ,
- Evaluate of EPA's Positive Matrix Factorization (PMF 5.0) model application for the combined mercury and $PM_{2.5}$ data set.

This scientific information is useful for better emissions control strategies and an improvement of the air quality and human health in New Jersey.

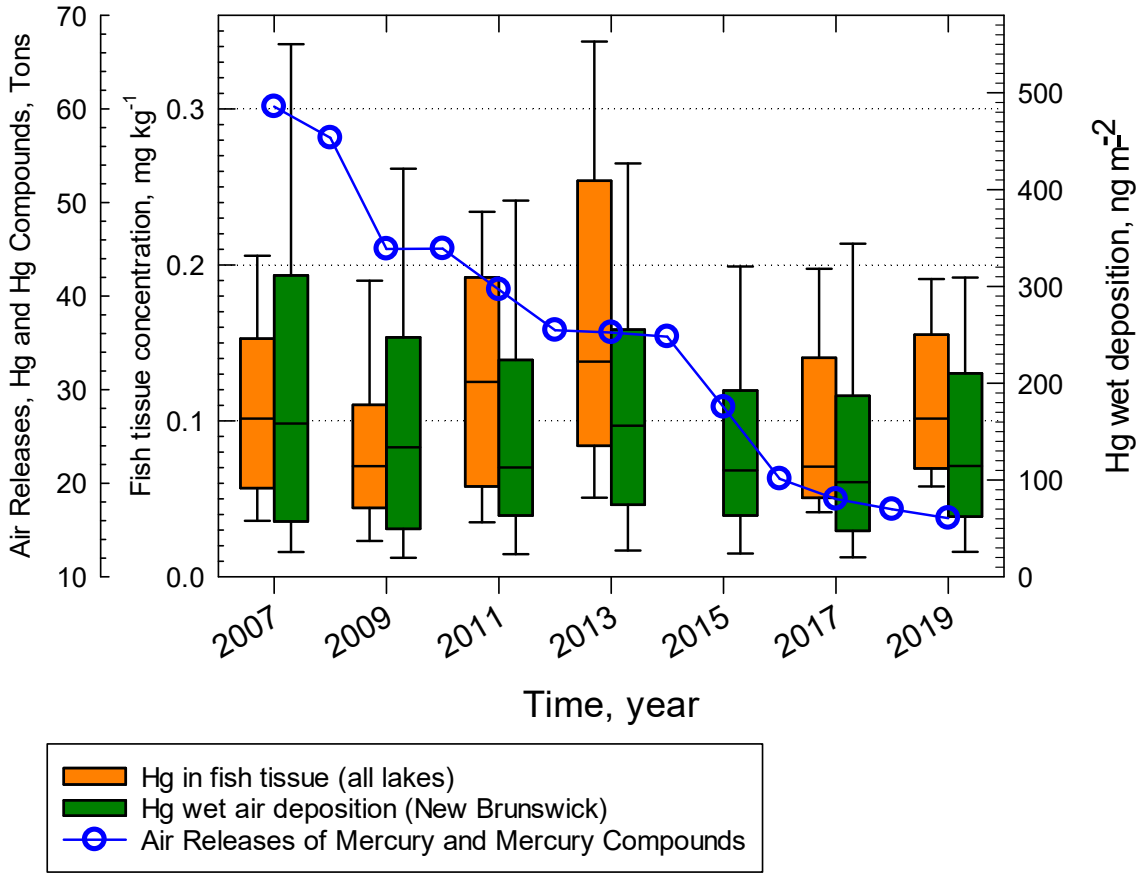

Fig. 1. Time series of the mercury concentration in fish tissue in New Jersey (Buchanan et al., 2023), mercury concentration in wet deposition measured in New Brunswick, New Jersey (Mercury Deposition Network, 1978-2023), as well as national air releases of mercury (EPA, 2023). While the emissions of mercury show a negative trend, concentrations of mercury in fish tissue and in wet deposition in New Jersey did not decline over this time period.

SAMPLING AND MEASUREMENTS

Aerosol sampling in Brigantine, New Jersey, (39.465 N, 74.4492 W, 5 m elevation) was conducted by NJDEP between September of 1991 and January of 2020 as a part of the Interagency Monitoring of PROtected Visual Environments (IMPROVE) network, a consortium of EPA and Federal land management agencies (Malm et al., 1994; Cahill et al., 1986).

The samples were analyzed by Particle Induced X-ray Emission (PIXE), Ion Chromatography (IC), and X-Ray Fluorescence (XRF) to determine particulate chemical composition, by proton elastic scattering analysis (PESA) for elemental hydrogen concentration, and by Thermal Optical Reflectance (TOR) method to measure elemental (EC1-EC3, OP) and organic carbon (OC1-OC4) fractions (Chow et al., 1993). A calibrated absorption coefficient was measured from a Teflon filter by using a hybrid integrating plate and sphere method (fAbs), and an uncalibrated absorption index was measured from a Teflon filter by using a laser integrating plate method (fAbs_HIPS). The samples of particles less than 2.5 μm in diameter were collected on filters for 24 hours every 3 days. The data set included gravimetric measurement of fine (MF) and total mass concentrations (MT), as well as calculated coarse mass (CM_calc), reconstructed fine mass (RCFM), soil, and sea salt, ammonium SO_4 and ammonium NO_3, elemental (EC) and organic (OC) carbon concentrations. Table 1 presents the summary for the reported data set. Table 2 describes the measured species.

A TEKRAN monitor was used by NJDEP for continuous hourly measurements of gaseous elemental mercury (GEM), particulate bound mercury (PBM), and gaseous oxidized mercury (GOM). The mercury data were averaged to correspond to the 24-hrs $PM_{2.5}$ concentrations data. The mercury measurements were performed from March of 2009 to June of 2014.

A total of 3,144 (samples) x 46 (parameters) =144,624 array of combined particulate and mercury data and corresponding array of error estimates were used for the PMF modeling for Brigantine, New Jersey.

FACTOR ANALYSIS

An advanced type of factor analysis, PMF (Paatero and Tapper, 1994), which utilizes error estimates of the data to provide an optimum data point scaling was used. PMF is a method based on solving the factor analysis problem by least-squares using a data point weighing method (Paatero, 1997). The solution was forced to be non-negative using a penalty function. The factor analysis model is given by

$$\boldsymbol{X} = \boldsymbol{A} \times \boldsymbol{B} + \boldsymbol{E}$$

Where $\boldsymbol{X}$ is a matrix of observed data, mode $\boldsymbol{A}$ is the unknown left-hand factor matrix (time series or source strength mode), mode $\boldsymbol{B}$ is the unknown right-hand factor matrix (chemical composition or source profile mode), and $\boldsymbol{E}$ is a matrix of residuals. The difference between the model and the data is

$$\boldsymbol{E = X - A \times B}$$

The model solves the least-squares problem by minimizing this difference and using a matrix of known estimated uncertainties for each x value. The details of the algorithm were reported by Paatero, 1997. The PMF 5.0 model software was provided by EPA (EPA, 2014).

The important advantage of the PMF method is the ability to handle missing and below detection limits data by adjusting the corresponding error estimates of these data points. It was especially essential for the Brigantine data set because data for some elements, such as chlorine (Cl), have over 60% of the values below limits of detection. Mercury (Hg) data was only measured in 2009-2014, and therefore about 90% of the mercury data can be considered as missing. Missing data and data below detection limits values were replaced by mean concentration and half of the detection limit values, respectively, and large error estimates were used for such values. PMF error estimates equal to 8 times the mean values were used for missing data points. The average detection limit was used for the error estimates for the values below the detection limit, so that the error estimates were equal to 200% of the values for these data. For the determined values, one should specify the effective error estimates so that they include all errors that produce a deviation between the fit and the observed value. Since different analytical methods were used and a variety of measured uncertainties were reported for different species/methods, for each measured data point a sum of the 8% of the data value and an average detection limit value, reported for the species, was used.

There is no simple rule for calculating error estimates. Analytical errors are only part of the total random error which is unknown. Data for some elements such as Cl, Al, Mg, Hg, etc. had either many values below the detection limits or missing values (Table 1). Therefore, further adjustments of the error estimates were necessary. The final set of the error estimates was obtained by running the PMF program many times with different sets of error estimates and applying the trial-and-error method until a substantially improved fit to the data was achieved. The quality of the model was evaluated by the analysis of the Q values (EPA, 2014), the frequency distributions of the residuals, the loading ratios for the sea salt and soil factors, and similar information from previous studies on chemical composition of emissions from known sources. Over 100 combinations of weight coefficients were tested for solutions with a different number of factors, and the most reasonable solution was chosen.

RESULTS AND DISCUSSION

Initial Data Investigations. A study of the time series and scatterplots is a useful tool of data analysis. It provides a helpful preliminary understanding of the possible sources of aerosol. The time series of major particulate species concentrations for Brigantine, NJ, are shown in Figures 2-4. Examples of scatterplots for the measured species concentrations are shown in Figures 5 and 6. Table 1 presents the summary of the data statistics.

Figures 2 and 3 show time series of the total fine mass $PM_{2.5}$ (MF) concentration and concentrations of species which likely represent different combustion sources. Aerosol elemental carbon (EC) and sulfur

(S) concentrations ranged from 0.0001 to 4.1 μg m^{-3} and from 0.005 to 8.02 μg m^{-3}, respectively, while the total fine aerosol mass concentration (MF) ranged from 0.3 to 106.8 μg m^{-3} (Figure 2 and 3).

The S and MF time series have maxima in summer and minima in winter (Figure 2). The summer increase in S is due in part to photochemical enhanced secondary sulfate formation. The $NO_3^=$ time series has maxima in winter and minima in summer (Figure 2). Time series of MF, S, and Se (Figure 2) show a negative trend over the period of measurements, likely related to reduction in coal consumption (Figure 1) and impact of the tighter air pollution regulations for power plants. No clear structure can be seen in the seasonal variations of elemental carbon but there is a decline in EC concentrations over the period of measurements (Figure 3). Several high pollution episodes (e.g., during the summer of 2002) can be seen simultaneously in the EC, OC1, and MF time series (Figures 2 and 3), suggesting the presence of woodsmoke particles from forest fires with a high organic matter content. Time series of soil species, Si and Al, show peaks in summer (Figure 3). They likely represent increased soil particles emission in the vicinity of the Brigantine site in summer. Time series of Ni, Pb and Zn (Figure 4) show a negative trend over the period of measurements. It is likely related to the recent tighter air pollution regulations on oil combustion (Ni), metal smelting and incineration (Pb, Zn). Copper (Cu) time series (Figure 4D) show no trend over the period of sampling.

Figures 5 and 6 show the Brigantine data scatterplots. They are useful for the qualitative study of the possible sources for different species. Higher data correlation for the MF vs S (R^2=0.75, Figure 5A), than for MF vs OC1 and MF vs EC on the scatter plots (Figures 5C and 5D, R^2=0.41 and R^2=0.45, respectively) could mean that sulfur is more associated with the fine mass, and both sulfur and fine mass are likely representing a single emission source. It was shown before (Song et al., 2001) that the coal combustion and the subsequent secondary sulfate aerosol formation from the source are the main contributors to the total fine mass in the Northeastern US. Since there is high correlation between MF and S data, the observation of the scatter plots on Figure 5A for Brigantine seems to confirm the earlier results on the coal combustion source of Song et al. (2001). The two sets of data points on the EC/S plot most likely represent two different sources of black carbon (Figure 5B). It has also been demonstrated (Polissar et al., 1996) that the ratio EC/S could be used for distinguishing between long distance and local combustion sources. Emissions with the high EC/S ratio generally represent wood burning, as well as exhaust from motor vehicles, incineration, and metal smelting (Olmez et al., 1988; Watson et al., 1994), while emissions with the lower EC/S ratio are associated with the coal combustion sources (Polissar et al. 2001).

Figure 6A shows the Se vs S scatterplot. Selenium (Se) is generally an important tracer for coal combustion (Olmez et al., 1988; Polissar et al. 2001), and the scatter plot likely shows that the set of the data points with the higher Se/S ratio is associated mainly with the coal combustion in winter, while the set with the lower Se/S ratio represents emissions from the coal combustion plus the enhanced photochemical secondary sulfate particles formation in summer. Figure 6A shows the two groups of data with the higher and lower Se/S ratios, which most likely represent emissions from these two sources both related to coal combustion.

The Zn/Pb, Cu/Zn and Al/Si scatterplots are shown in Figures 6B, C, and D. The scatter plots show that most likely there are common sources of zinc (Zn), lead (Pb), and copper (Cu). These elements are usually emitted by metal smelting and incineration (Olmez et al.,). Al and Si are the soil elements. High

correlation for the Al and Si concentrations on the scatter plot of Figure 6D most likely represents the same for these elements soil emission sources.

TABLE 1. Arithmetic means (MEAN), Medians (MED), Maximum Concentrations (MAX), Standard Deviations (STD), percentages of missing, below detection limits (DL), and measured data. Descriptions of the parameters and units presented in Table 2 (Federal Land Manager Environmental Database, 2023)

Parameter	MEAN	MED	MAX	STD	% MISSING	% BELOW DL	%MEASURED
AL	0.026	0.014	0.928	0.048	0.859	30.280	68.861
ammNO3	1.054	0.643	21.811	1.184	16.476	0.000	83.524
ammSO4	4.097	2.840	77.855	4.249	0.700	0.000	99.300
AS	0.000	0.000	0.006	0.000	0.827	33.969	65.204
BR	0.003	0.003	0.041	0.002	0.827	0.095	99.078
CA	0.027	0.023	0.292	0.017	0.859	0.127	99.014
CL	0.059	0.002	2.538	0.219	0.859	59.606	39.536
CHL	0.169	0.062	3.590	0.377	5.471	15.267	79.262
CM_calc.	9.480	6.982	136.478	9.223	6.234	0.095	93.670
CR	0.000	0.000	0.011	0.001	0.859	34.796	64.345
CU	0.001	0.001	0.042	0.001	0.827	3.912	95.261
EC	0.393	0.342	4.123	0.280	3.181	0.127	96.692
EC1	0.575	0.499	11.866	0.442	3.181	0.032	96.788
EC2	0.057	0.047	0.444	0.038	3.181	2.290	94.529
EC3	0.012	0.012	0.220	0.010	3.181	67.112	29.707
fAbs	3.441	3.290	20.520	1.836	38.295	0.254	61.450
fAbs_HIPS	540.622	515.260	1872.500	244.679	46.851	0.223	52.926
FE	0.032	0.027	0.414	0.027	0.827	0.032	99.141
H	0.466	0.385	5.651	0.328	34.001	0.032	65.967
K	0.041	0.035	0.915	0.030	0.859	0.000	99.141
MF	8.790	7.215	106.793	6.234	1.113	0.064	98.823
MG	0.024	0.013	0.342	0.031	0.859	48.855	50.286
MN	0.001	0.001	0.012	0.001	0.859	18.321	80.821
MT	18.331	15.357	144.076	12.312	5.280	0.000	94.720
N2	0.014	0.014	0.171	0.021	2.449	29.008	68.543
NA	0.217	0.127	2.949	0.277	0.859	16.253	82.888
NI	0.001	0.001	0.012	0.001	0.827	4.835	94.338
NO3	0.803	0.501	16.908	0.886	2.449	0.000	97.551
OC	1.492	1.242	55.983	1.413	3.181	0.032	96.788
OC1	0.090	0.044	2.075	0.150	3.181	21.565	75.254
OC2	0.327	0.264	12.657	0.326	3.181	0.032	96.788
OC3	0.431	0.330	19.683	0.482	3.181	0.064	96.756
OC4	0.400	0.293	13.258	0.395	3.181	0.032	96.788
OP	0.245	0.205	8.310	0.277	3.181	6.234	90.585
P	0.002	0.002	0.042	0.002	0.859	79.707	19.434

PB	0.002	0.002	0.028	0.002	0.827	3.276	95.897
RB	0.000	0.000	0.004	0.000	0.827	48.346	50.827
RCFM	8.442	6.991	111.736	5.879	20.038	0.000	79.962
S	0.994	0.723	8.023	0.886	0.859	0.000	99.141
SE	0.001	0.001	0.008	0.001	0.827	2.481	96.692
SeaSalt	0.298	0.104	6.461	0.662	0.732	14.695	84.574
SI	0.084	0.058	1.680	0.101	0.859	1.972	97.169
SO4	2.916	2.033	56.622	3.020	2.449	0.000	97.551
SOIL	0.393	0.298	7.795	0.429	0.859	0.000	99.141
SR	0.000	0.000	0.008	0.000	0.827	9.478	89.695
TI	0.004	0.002	0.060	0.005	0.859	7.156	91.985
V	0.002	0.001	0.024	0.003	0.859	11.387	87.754
ZN	0.007	0.005	0.064	0.006	0.827	0.159	99.014
ZR	0.000	0.000	0.003	0.000	0.827	63.104	36.069
Avg GEM	1.385	1.349	4.184	0.388	89.218	0.000	10.782
Avg PBM	5.880	3.679	129.658	10.670	89.377	1.590	9.033
Avg GOM	1.630	0.754	14.242	2.489	89.377	1.908	8.715

PMF results. Results of the PMF analysis are presented in Figures 7 - 14. Figure 7 represent factor fingerprints, while figures 8 and 9 represent source profiles and Figures 10 and 11 show corresponding time series for the factors F1-F12. The factor (source) F1 represents nitrate-rich secondary particulates from combustion sources (Figures 7, 8 and 10). It has high loadings of $NO_3^=$. Concentrations of particles emitted from this source have seasonal variation with maxima in winter (F1, Figure 10). These high concentrations in winter are, most likely, caused by the frequent temperature inversions which occur in Brigantine in winter. This source F1 accounts for about 7.8% of the total $PM_{2.5}$ mass concentration (Figure 12). The previous Brigantine aerosol studies of Song et al. (2001), and Kim and Hopke (2004) estimated 8% and 6% nitrate-rich secondary particulates contributions to the $PM_{2.5}$ mass concentrations, respectively.

The soil factor F2 has the highest loading for Al and Si (Figures 7 and 8). This factor has also high loadings of Ca, Fe, Ti, and calculated soil (SOIL, Figure 8). The ratio Al/Si for the soil factor F2 is equal to 0.79. This ratio is about 2.7 times higher than for the average earth crust (0.293) (Mason, 1966). However, this value agrees well with the properties of the original data: the slope for the linear regression fits for the Al/Si scatterplot is also higher than the average crust Al/Si ratio (Figure 6D). The time variations of the soil factor F2 have peaks in the summer that corresponds to the likely higher rates of soil emission in the summer (F2, Figure 10). Episodes of high soil concentrations are, most likely, related to local traffic activity near the sampling site. Probably, both local and long-distance sources of soil aerosol are related to the soil factor. The Brigantine site was occasionally impacted by the distant Sahara dust storms (Hopke and Kim, 2004). The long-range Sahara dust transport to the US was reported by Gerbhart et al., 2001; Lamancusa and Wagstrom, 2019. An example of the backward trajectory plot, obtained by the HYSPLIT model (HYSPLIT, 2015) for a day, when the soil factor contribution was high (source F2, Figure 10), presented in Figure 15. It shows the Sahara dust transport episode event. Source F2 contributes 2% to the $PM_{2.5}$ mass concentration (Figure 12). The previous

Brigantine studies reported 1% (Song et al., 2001) and 2% (Lee et al., 2002) contributions of the soil particulate mass to the $PM_{2.5}$ mass concentration.

Factor F3 has high loadings of As, Cr, Cu, elemental carbons, absorption coefficients, and elemental mercury (Figures 7 and 8). It has been identified by PMF as an As-rich coal combustion source, but it can also represent emissions from arsenic (As) smelting facilities. It may indicate transport from a large smelter located near Noranda at the Quebec/ Ontario border, reported in (Loranger and Zayed, 1994; Polissar et al., 2001). Concentrations of particles emitted from this source have seasonal variation with maxima in winter and clear negative trend (F3, Figure 10). The negative trend can be explained by the decline in emissions from coal combustion and smelting activities. Source F3 contributes only 1.1% to the $PM_{2.5}$ mass concentration (Figure 12) but, according to the PMF model, 43.8% of elemental mercury (GOM), 24.6% of particulate mercury (PBM), and 13% of gaseous oxidized mercury (GOM), measured in Brigantine, are transported from this source (Figure 12).

Factor F4 represents the coarse particulate mass. Besides calculated coarse mass CM, this factor has high loadings of some soil elements, such as Al, Fe, Mn, and Ti (Figures 7 and 8). Time series of F4 have peaks in the summer that corresponds to likely coarse soil particles contribution (F4, Figure 10).

Factor F5 has the highest loadings of pyrolyzed carbon fraction OP (Figures 7 and 8). It also has high loadings of EC1, OC2, OC and P (Figure 8). Most likely this factor represents emissions from mixed combustion sources, including mobile sources, and photochemical particle formations. Highest concentration was observed on July 7, 2002, when the smoke from Canadian forest fires was transported to the Northeastern USA (Colarco et al., 2004). It can also represent diesel emissions, since it has high loadings of EC1 and OP (Kim and Hopke, 2004). Source F5 contributes 10.6% to the $PM_{2.5}$ mass concentration (Figure 12). No clear structure of an annual cycle in the seasonal variations for this factor is observed (F5, Figure 10).

The sea salt factor F6 has high loadings of Ca, Cl, Mg, Na, and Sr (Figures 7 and 8). This factor was obtained despite the large number (60%, Table 1) of below detection limit values for Cl concentrations (Table 1). Cl/ Na loading ratios for the sea salt factor and for the seawater are 1.53 and 1.80, respectively. This factor most likely represents sea salt emissions from the Atlantic Ocean and emissions of the road salt from the areas near the sampling site in winter. Concentrations from this source do not show a clear seasonal pattern (F6, Figure 10). The sea-salt factor F6 provides 6% of the $PM_{2.5}$ mass concentration (Figure 12).

Another combustion factor F7 has the highest loadings of nickel (Ni) and vanadium (V) (F7 on Figures 7 and 9). This source is suggested to represent emissions from oil-fired power plants located on the east coast of the United States. The combustion of heating oil might also play a role in contributing to this source. The Ni/V ratio was equal to 0.94 for this factor, and it is close to 0.95, a reported ratio for an oil-fired power plant (Omez et al., 1988). Higher concentrations during winter/spring for the oil factor are observed (F7, Figure 11). Concentrations for this factor show a significant negative trend over the time interval of sampling. This negative trend suggests a major reduction in oil-fired power plant emissions during the period from 1991 to 2020. This source provides 1.7% of the $PM_{2.5}$ mass concentration (Figure 12). Previous Brigantine aerosol studies estimated 1% (Kim and Hopke, 2004), 2% (Song et al., 2001) and 4% (Lee et al., 2002) oil combustion contributions to the $PM_{2.5}$ mass concentration.

The factor F8 with high loading of Zn also has the highest loadings of Cu, Fe, Mn, Ni, and GOM (Figures 7 and 9). This factor may indicate emissions from some smelting of nonferrous metal ores. The seasonal pattern has higher concentrations in winter (F8, Figure 11). This factor for accounts 0.9% of the total $PM_{2.5}$ mass concentration (Figure 12). Time series don't show any trend.

The factor F9 has high loadings of organic carbon OC and its fractions OC1-OC4 (Figure 9). There is no clear seasonal pattern for the time series of this source (F9, Figure 11). It represents mixed combustion emissions from different activities, such as wood, coal combustion, and automotive exhaust. Previous Brigantine study showed organic and elemental carbon fractions can be used to resolve diesel and gasoline emissions (Kim and Hopke, 2004). This study included data for a much longer period, resulted in different results and several different sources. Factor F9 accounts for 14.4% of the total $PM_{2.5}$ mass concentration (Figure 12).

The PMF solution also contained a factor F10 with high loadings of Cr, Pb, and Zn (Figures 7 and 9). The high Zn and Pb loadings for the factor could arise from several types of sources. Probable sources include municipal waste incineration and nonferrous metal smelting. The time series for the Zn-Pb factor has visual negative trend which is most likely related to reduced emissions in 2000s (F10, Figure 11). Source F10 contributes 1.8% to the $PM_{2.5}$ mass concentration (Figure 12). The previous Brigantine aerosol studies estimated 2% (Kim and Hopke, 2004), 5% (Song et al., 2001 and Lee et al., 2002) contributions of similar sources to the $PM_{2.5}$ mass concentration.

The factor F11 with high loadings of hydrogen (H), selenium (Se), sulfur (S), and organic carbons (OCs) has the annual cycle with the summer maxima (Figures 7, 9 and 11). It is suggested that this factor represents the photochemically enhanced sulfate production from SO_2 in the summer from emissions of the coal fired power plants. There could also be secondary sulfate production from heterogeneous processes in cloud water and fog. Sources, related to F11, provide the highest contribution to fine particulate mass concentrations equal to 40% (Figure 12). Earlier, Kim and Hopke (2004) reported 48% for the sulfate factor contribution to $PM_{2.5}$ for Brigantine but emissions from the coal power plants declined after their work was published, which can be seen in Figure 11 (F11). It was shown that the coal combustion factors represent emissions from the source areas extending from the lower Great Lakes to the south of the Ohio River Valley, encompassing the locations of many large electricity-generating plants and industrial sources in the Midwest (Kim and Hopke, 2004; Polissar et al., 2001).

The woodsmoke factor F12 has high loadings of black carbon (BC), hydrogen (H), and potassium (K) (Figure 7 and 9). This factor is attributed to particles from local wood smoke and possibly from other related combustion sources. The ratio of the BC to S loadings for the woodsmoke factor corresponds well to a reported ratio for wood combustion (Polissar et al., 2001). The time series for the woodsmoke factor F12 has maxima in the winter/spring season and minima in the summer (Figure 11) representing higher emissions of wood smoke or/and more effective transport of soot from sources to the sampling site in winter. The time series also shows several high spikes during summers, indicating smoke from several forest fires and fireworks.

Thus, twelve sources of air pollution have been identified by PMF, such as coal and oil combustion, incineration/metal production, wood combustion, soil, sea salt emissions, etc. The pattern of source contributions shows a predominant sulfate source F11 with a strong summer peak. 40% of the total fine mass was contributed by this source. The largest contributions to $PM_{2.5}$ were from primary and

secondary coal and mixed combustion sources F11 (40%), F9 (14.4%), and F5 (10.6%) (Figure 12). On average more than 60% of the total $PM_{2.5}$ was emitted from these sources (MF on Figure 12).

The main sources of gaseous elemental mercury (GEM) and gaseous oxidized mercury (GOM) in Brigantine are the coal combustion source F3 (43.8%) and smelting/mixed combustion source F8 (57.2%), respectively (Figure 12). Particulate bound mercury (PBM) was emitted by a variety of sources – such as mixed combustion F9 (28.5%), coal combustion F3 (24.6%), wood combustion F12 (24.8%), and oil combustion F7 (18.3%) sources (Figure 12). Main source F3 of gaseous elemental mercury (GEM) showed a negative trend (Figure 10). The assumption is that since mercury is emitted from different sources, including those outside of New Jersey, the wet deposition levels of mercury in New Jersey did not decrease.

Figures 13 and 14 represent sources, obtained by PMF, for different aerosol species. Sources of zinc (ZN), selenium (SE), organic and elemental carbons (OC and EC), identified by the Positive Matrix Factorization for Brigantine, New Jersey, are shown in Figure 13. Major sources of ZN are smelting (F8, 40.4%) and incineration (F10, 32.6%). Main sources of SE are incineration (F10, 20.1%) and coal combustion (F11, 44.8%). Organic carbon (OC) was mostly associated with the combustion sources F5, F9, and F11 (27.1%, 38.7%, and 10%, respectively (Figure 13). Major sources of elemental carbon (EC) are coal combustion source F3 (52.8%), combustion sources F5 (12.7%) and F11 (11.9%).

Light absorption coefficient (fAbs) was mostly associated with the coal combustion source F3 (46.7%) (Figure 14). 75.5% of $AmmSO_4$ and 84.7% of lead (PB) are the emissions from the coal combustion source F11 and incineration source F10, respectively (Figure 14). Finally, sources of potassium are F5 (13.2%), F9 (19.3%), and F12 (47.1%).

SUMMARY

- Emissions from different anthropogenic activities and secondary aerosol production are the major sources of the aerosol measured in Brigantine, New Jersey.
- Twelve sources of air pollution have been identified by PMF, such as coal and oil combustion, incineration/metal production, wood combustion, soil, and sea salt emissions, etc.
- The Midwestern coal combustion (F11) was identified as a major source for PM2.5 in New Jersey (40%). About 65% of total fine mass (PM2.5) in Brigantine are the emissions from the three major combustion sources F5, F9, and F11.
- Contributions from the three sources – F7 (Oil Combustion, V-Ni), F10 (Incineration/Metal Production, Pb-Zn), and F11 (Coal Combustion, SO4=) - showed negative trends.
- The main source of the gaseous elemental mercury (GEM) is coal combustion (F3, As-EC), while the main source of GOM is metal smelting F8 (Cu-Zn). Emissions of particulate mercury (PBM) are related to the coal combustion source F3 (As-EC) and three other combustion sources F7, F9, and F12.

- The use of the EPA PMF receptor model is an effective approach of the identification of the air pollution sources.

FUTURE RESEARCH

It is recommended to update the data set, include recent $PM_{2.5}$ measurements, and repeat the PMF modeling runs to study the recent changes in the air pollution and sources, related to reduced economic activities in 2020-2023. Conducting the PMF modeling for various time periods would also provide valuable insights into changes in sources and their impacts over time. It is also recommended to perform a similar study for the NJDEP sampling site in New Brunswick, where both the mercury and $PM_{2.5}$ data are available. It would be also useful to study the mercury data from the Mercury Deposition Network, including the very recent data, to identify trends, sources, and geographical locations of the possible sources. Employing the Potential Source Contribution Function (PSCF) model could offer insights into probable geographical locations of sources identified through PMF analysis.

ACKNOWLEDGEMENTS

The author acknowledges Katrina Angarone, Nick Procopio, Lori Lester, Gary Buchanan, Mingzhu Fang from the Division of Science and Research for their support of the project, Olga Boyko, Luis Lim, and Rudy Zsolway from the Air Program for their help with the data, Robin Heston-Murphy and the Mercury Workgroup for their help with the important information on mercury sources.

REFERENCES

Buchanan G. A., Ruppel, B., Millemann, D., Polissar, A.V., 2023. Long-term Mercury project. (Unpublished results, NJDEP report in preparation).

Cahill, T.A., Eldred, R.A., Feeney, P.J., 1986. Particulate monitoring and data analysis for the National Park Service 1982-1985. NPS Contract USDICX-3-0056. U.S. Government Printing Office, Washington, DC.

Chow, J. C., Watson, J.G., Pritchett, L.C., Pierson, W.R., Frazier C.A., Purcell, R.G., 1993. The DRI thermal/optical reflectance carbon analysis system: description, evaluation, and applications in U.S. air quality studies. Atmospheric Environment 27, 1185-1201.

Colarco, P.R., Schoeberl, M. R., Doddridge, B.G., Marufu, L.T., Torres O., Welton, E.J., 2004. Transport of smoke from Canadian forest fires to the surface near Washington, D.C.: injection, height, entrainment, and optical properties. Journal of Geophysical Research 109, D06203, doi:10.1029/2003JD004248.

EPA, 2014. Positive Matrix Factorization Model for Environmental Data Analyses. https://www.epa.gov/air-research/positive-matrix-factorization-model-environmental-data-analyses

EPA, 2023. Mercury Air Releases Trends. https://www.epa.gov/trinationalanalysis/mercury-air-releases-trend

Federal Land Manager Environmental Database, 2023. https://views.cira.colostate.edu/fed/QueryWizard/Default.aspx

Gebhart K.A., Kreidenweis S.M., Malm W.C., 2001. Back-trajectory analyses of fine particulate matter measured at Big Bend National Park in the historical database and the 1996 scoping study. Science of The Total Environment 276, 185-204.

Hopke, P.K., 1991. An Introduction to receptor modeling. Chemometrics and Intelligent Laboratory Systems 10, 21-43.

Kim, E., Hopke, P.K, 2004. Improving source identification of fine particles in a rural northeastern U.S. area utilizing temperature-resolved carbon fractions. Journal of Geophysical Research 109, D09204.

Lamancusa, C., Wagstrom, K., 2019. Global transport of dust emitted from different regions of the Sahara. Atmospheric Environment 214, 116734

Lee, J.H., Yoshida, Y., Turpin, B.J., Hopke, P.K., Poirot, R.L., Lioy, P.J., Oxley, J.C., 2002. Identification of sources contributing to the Mid-Atlantic regional aerosol. Journal of Air & Waste Management Association 52, 1186-1205.

Loranger, S., Zayed, J., 1994. Manganese and lead concentrations in ambient air and emission rates from unleaded and leaded gasoline between 1981 and 1992 in Canada – a comparative study. Atmospheric Environment 28, 1645-1651.

Malm, W.C., Sisler, I.F., Huffman, D., Eldred, R.A., Cahill, T.A.J.,1994. Spatial and seasonal trends in particle concentration and optical extinction in the United States, Journal of Geophysical Research 99, 1347-1370.

Mason, B., 1966. Principles of Geochemistry, 3rd ed., John Wiley & Sons, New York.

Mercury Deposition Network, 1978-2023. Site NJ30, National Atmospheric Deposition Program. https://nadp.slh.wisc.edu/sites/mdn-NJ30/

NOAA, 2015. HYSPLIT trajectories. https://www.ready.noaa.gov/HYSPLIT_traj.php

Olmez, I., Sheffield, A.E., Gordon, G.E., Houck, J.E., Pritchett, L.C., Cooper, J.A., Dzubay, T.G., Bennett, R.L., 1988. Compositions of particles from selected sources in Philadelphia for receptor modeling applications. Journal of Air & Waste Management Association 38, 1392-1402.

Paatero, P., 1997. Least squares formulation of robust nonnegative factor analysis. Chemometrics and Intelligent Laboratory Systems 37, 15-35.

Paatero, P.; Tapper U., 1994. Positive matrix factorization: A non-negative factor model with optimal utilization of error estimates of data values. Environmetrics 5, 111-126.

Polissar A.V., Hopke, P.K., Malm W.C., Sisler J. F., 1996. The ratio of aerosol optical absorption coefficients to sulfur concentrations, as an indicator of smoke from forest fires when sampling in polar regions. Atmospheric Environment 30, 1147-1157.

Polissar A.V., Hopke, P.K., Poirot, R., 2001. Atmospheric aerosol over Vermont: chemical composition and sources. Environmental Science and Technology 35, 4604-4621.

Song, X.-H., Polissar, A.V., Hopke P.K., 2001. Sources of fine particle composition in the northeastern US, Atmospheric Environment 35, 5277-5286.

Watson, J.G., Chow, J.C., Lowenthal, L.C., Pritchet, C.A., Frazier, C.A., Neuroth, G.R., Robbins, R., 1994. Differences in the carbon composition of source profiles for diesel- and gasoline-powered vehicles, Atmospheric Environment 28, 2493-2505.

Weiss, P., Gay, D.A., Brigham M.E., Parsons M.T., Gustin, M.S., A.T. Schure, 2016. Trends in mercury wet deposition and mercury air concentrations across the U.S. and Canada, Science of The Total Environment 568, 546-556.

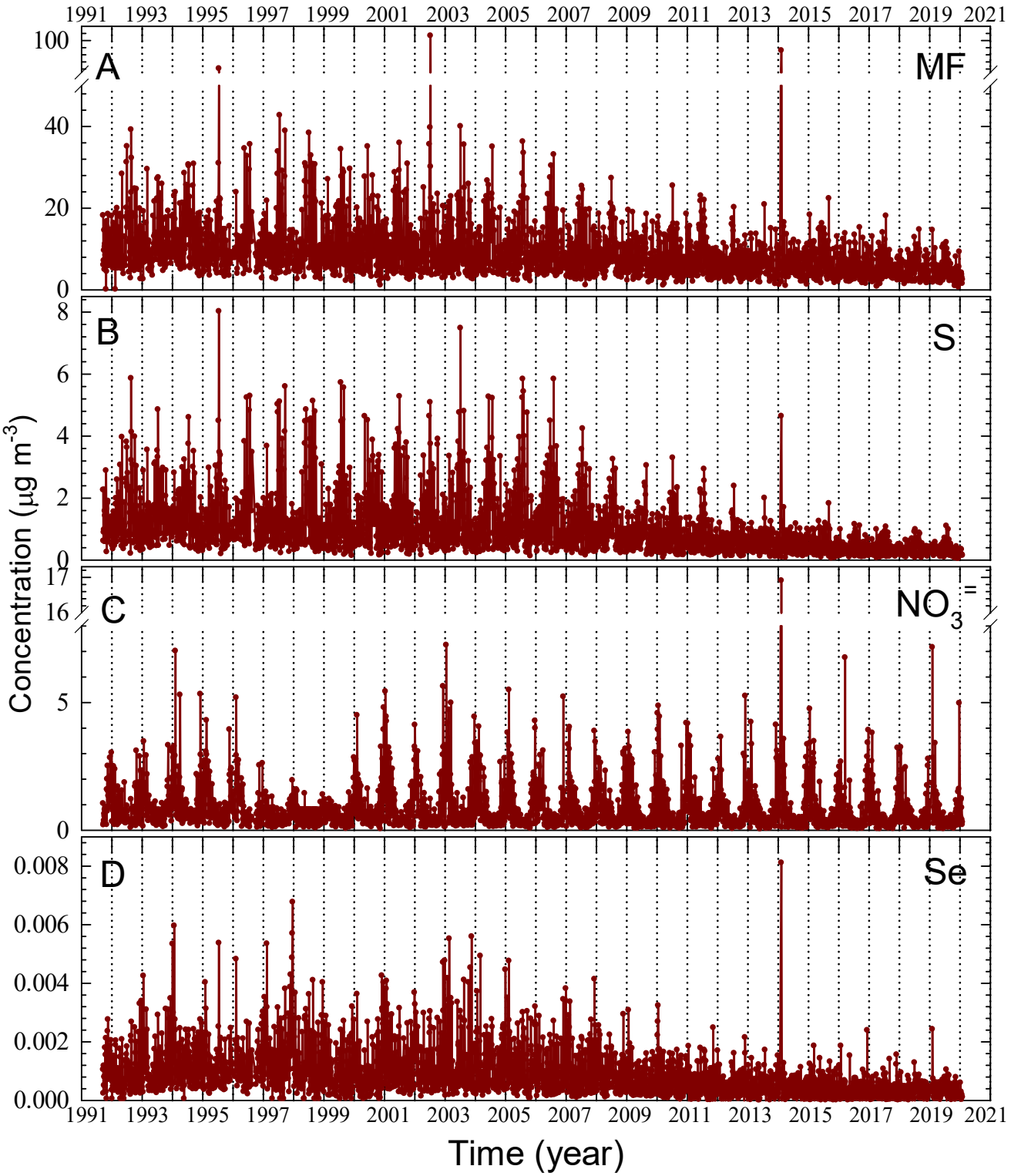

Fig. 2. Time series of air concentrations of MF ($PM_{2.5}$ or Particulate Matter less than 2.5 μm in diameter) (A), S (B), $NO_3^=$(C), and Se (D), measured in Brigantine, New Jersey. The samples of particles less than 2.5 μm in diameter were collected on filters for 24 hours every 3 days.

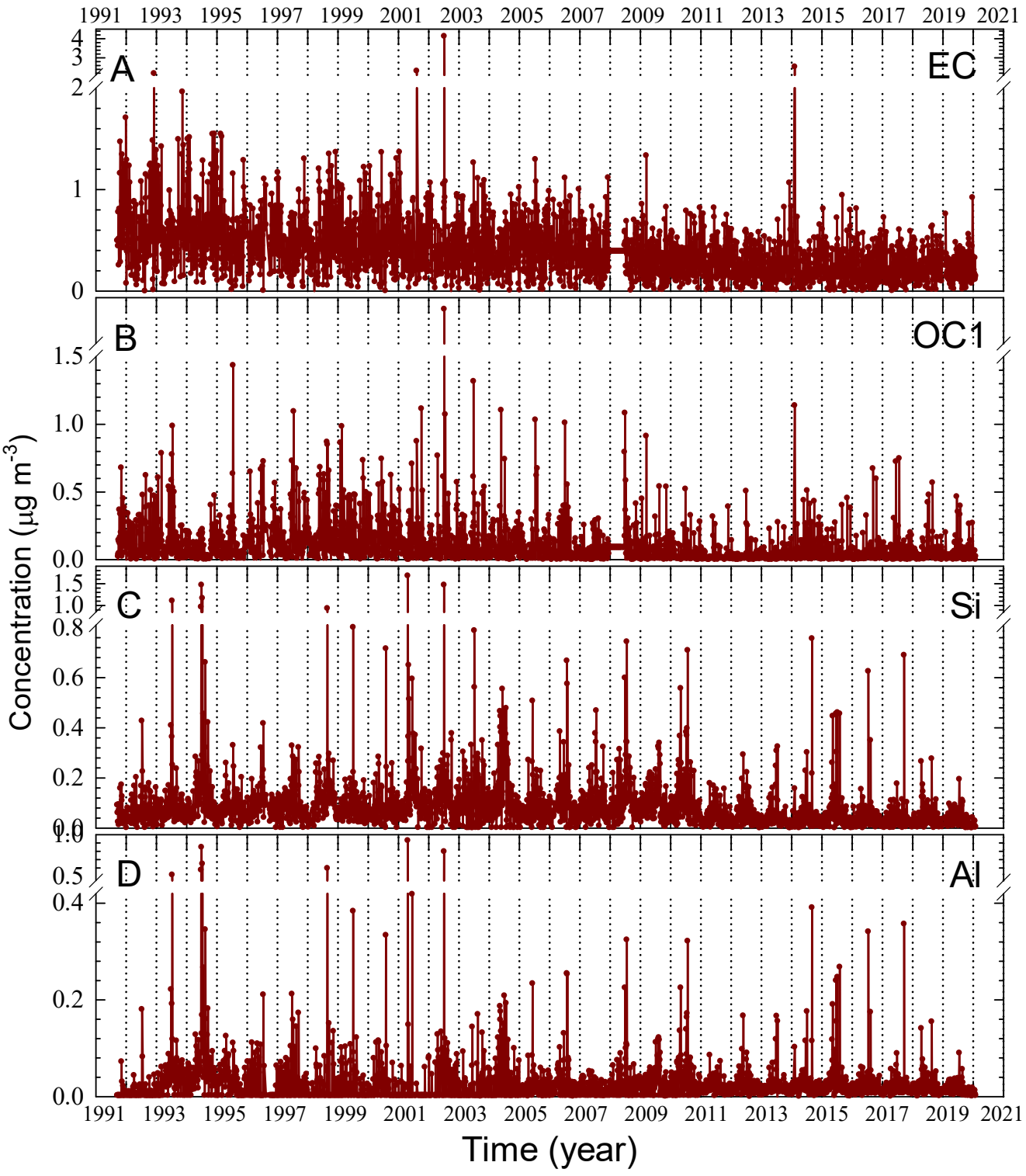

Fig. 3. Time series of air concentrations of EC (Elemental Carbon) (A), OC1 (Organic Carbon) (B), Si (C), and Al (D), measured in Brigantine, New Jersey. The samples of particles less than 2.5 μm in diameter were collected on filters for 24 hours every 3 days.

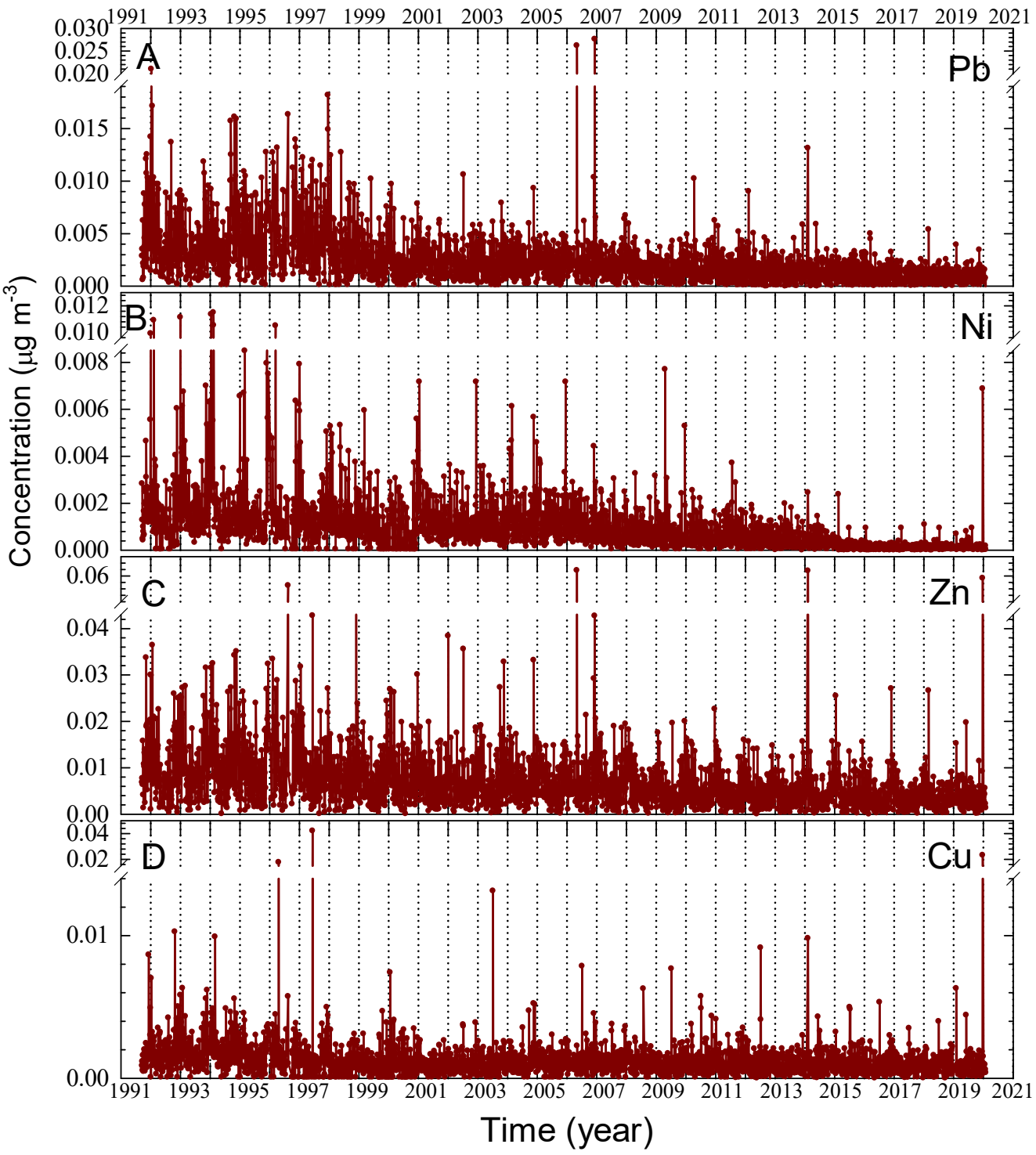

Fig. 4. Time series of air concentrations of Pb (A), Ni (B), Zn (C) and Cu (D), measured in Brigantine, New Jersey. The samples of particles less than 2.5 μm in diameter were collected on filters for 24 hours every 3 days.

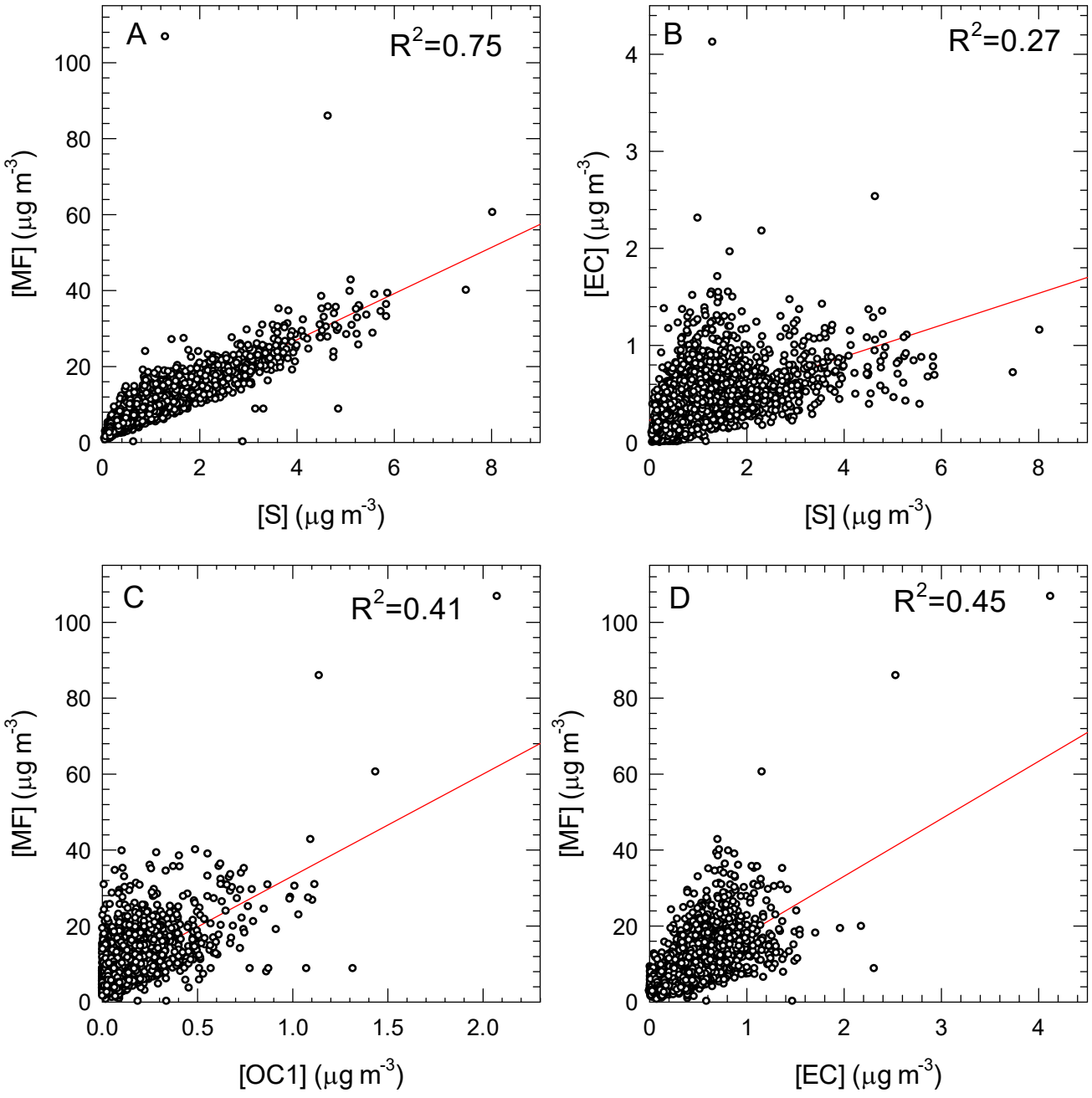

Fig. 5. Concentrations of particulate fine mass (MF) vs S (A); elemental carbon (EC) vs S (B); particulate fine mass (MF) vs organic carbon (OC1) (C); and particulate fine mass (MF) vs elemental carbon (EC) (D) for Brigantine, New Jersey. Red lines and corresponding squared correlation coefficients represent linear regression fits.

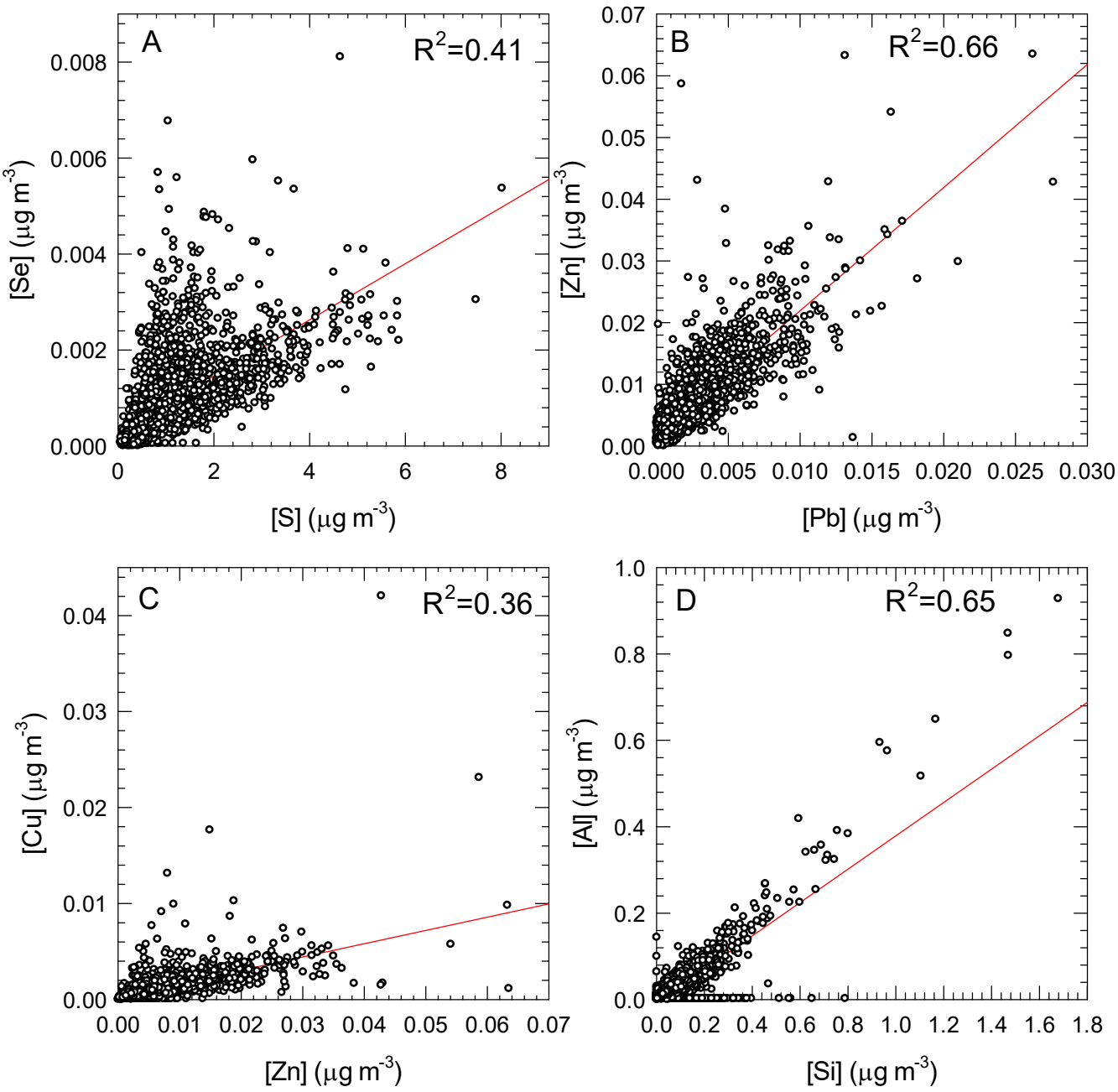

Fig. 6. Concentrations of Se vs S (A); Zn vs Pb (B); Cu vs Zn (C); and Al vs Si (D) for Brigantine, New Jersey. Red lines and corresponding squared correlation coefficients represent linear regression fits.

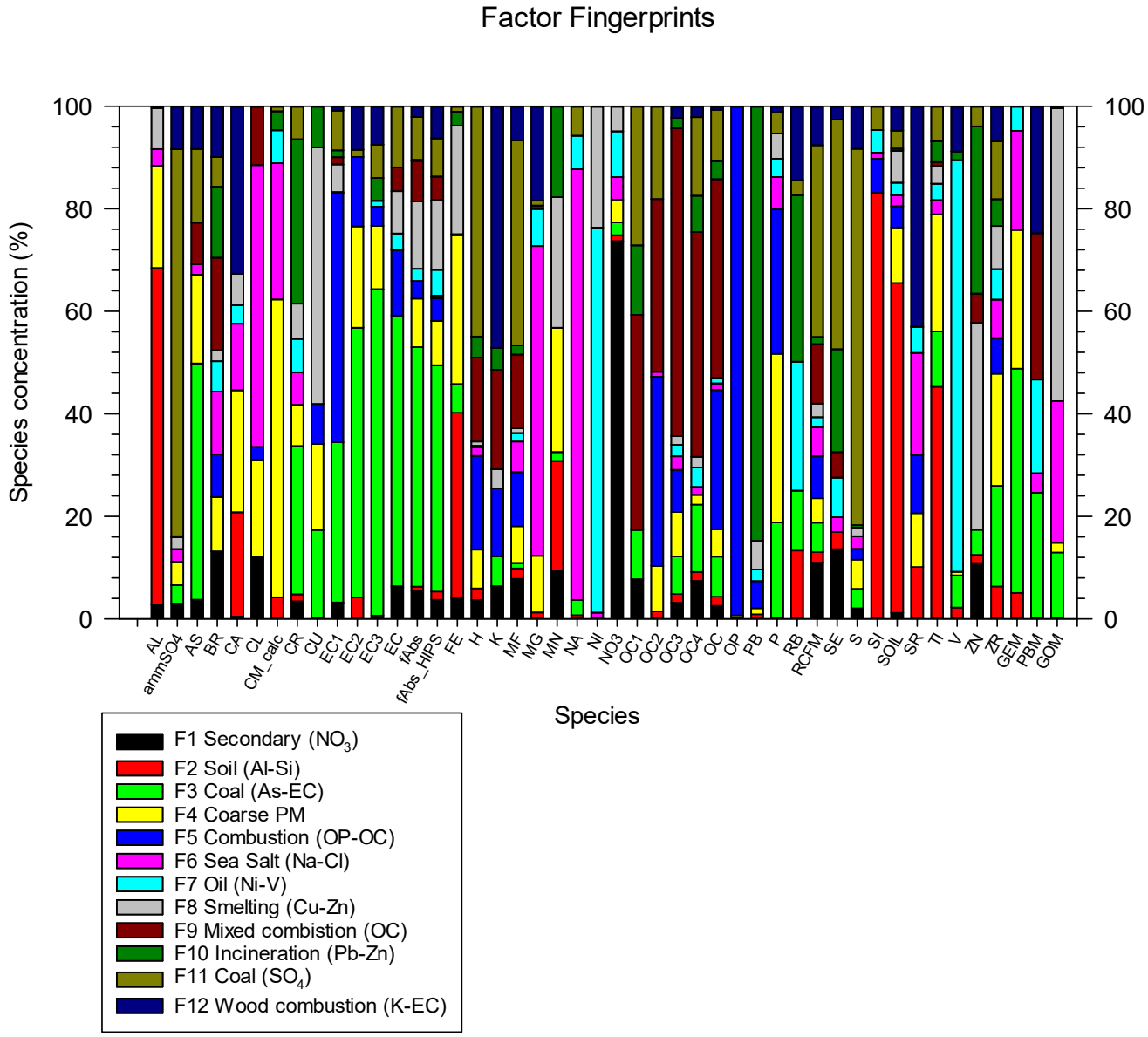

Fig. 7. Factors' fingerprints for the 12 sources of aerosol and mercury, resolved by the Positive Matrix Factorization (PMF) for Brigantine, New Jersey. The results were normalized, so that the sum of each parameter contributions over all sources was set equal to 100%. The list of parameters and their descriptions are presented in Table 2.

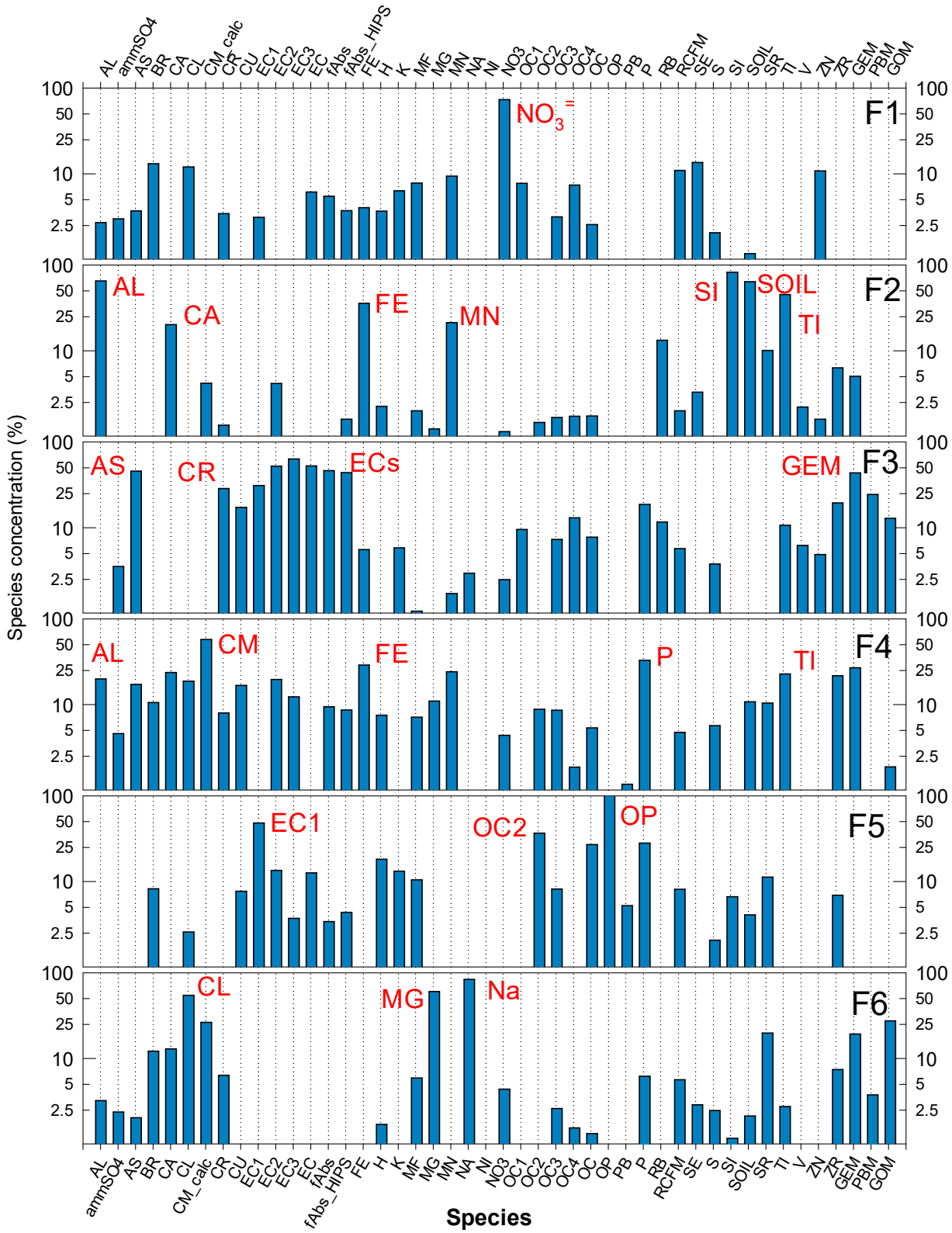

Fig. 8. Source profiles (Mode *B*) of aerosol and mercury species in the factors F7-F12, obtained by the Positive Matrix Factorization (PMF) for Brigantine, New Jersey. Red labels represent species with high loadings.

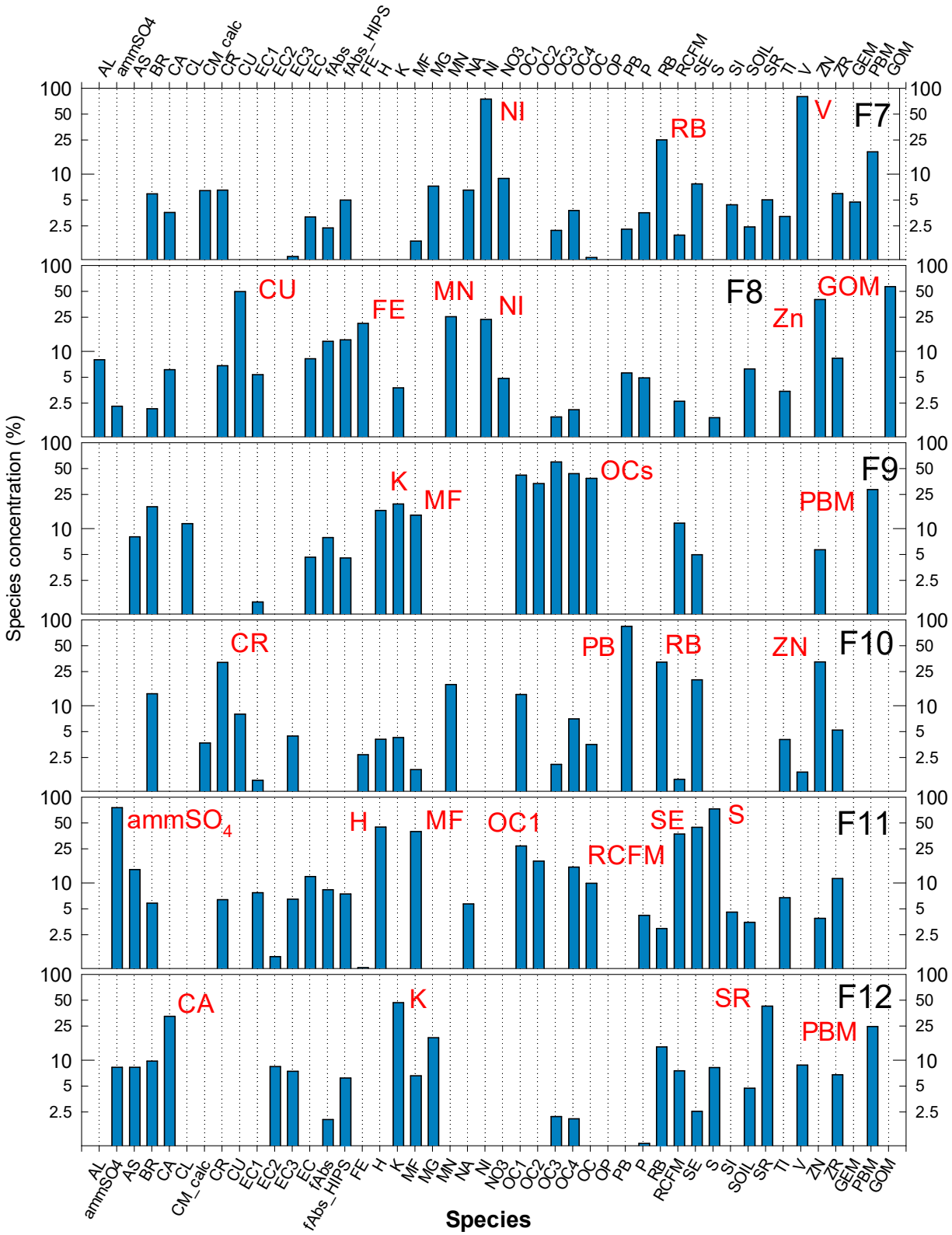

Fig. 9. Source profiles (Mode *B*) of aerosol and mercury species in the factors F7-F12, obtained by the Positive Matrix Factorization (PMF) for Brigantine, New Jersey. Red labels represent species with high loadings.

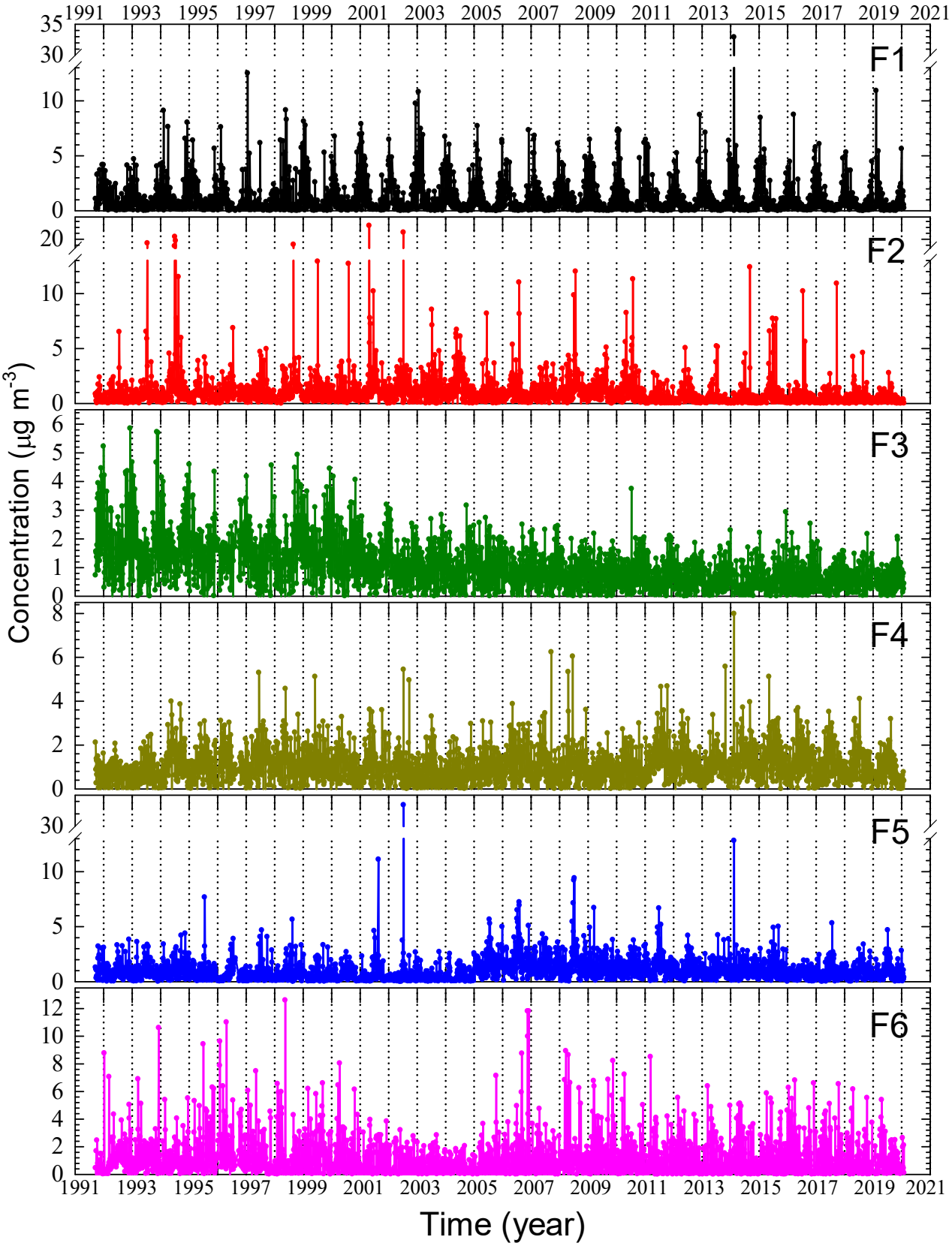

Fig. 10. Temporal variations (Mode *A*) of the factors F1-F6, obtained by the Positive Matrix Factorization (PMF) for Brigantine, New Jersey

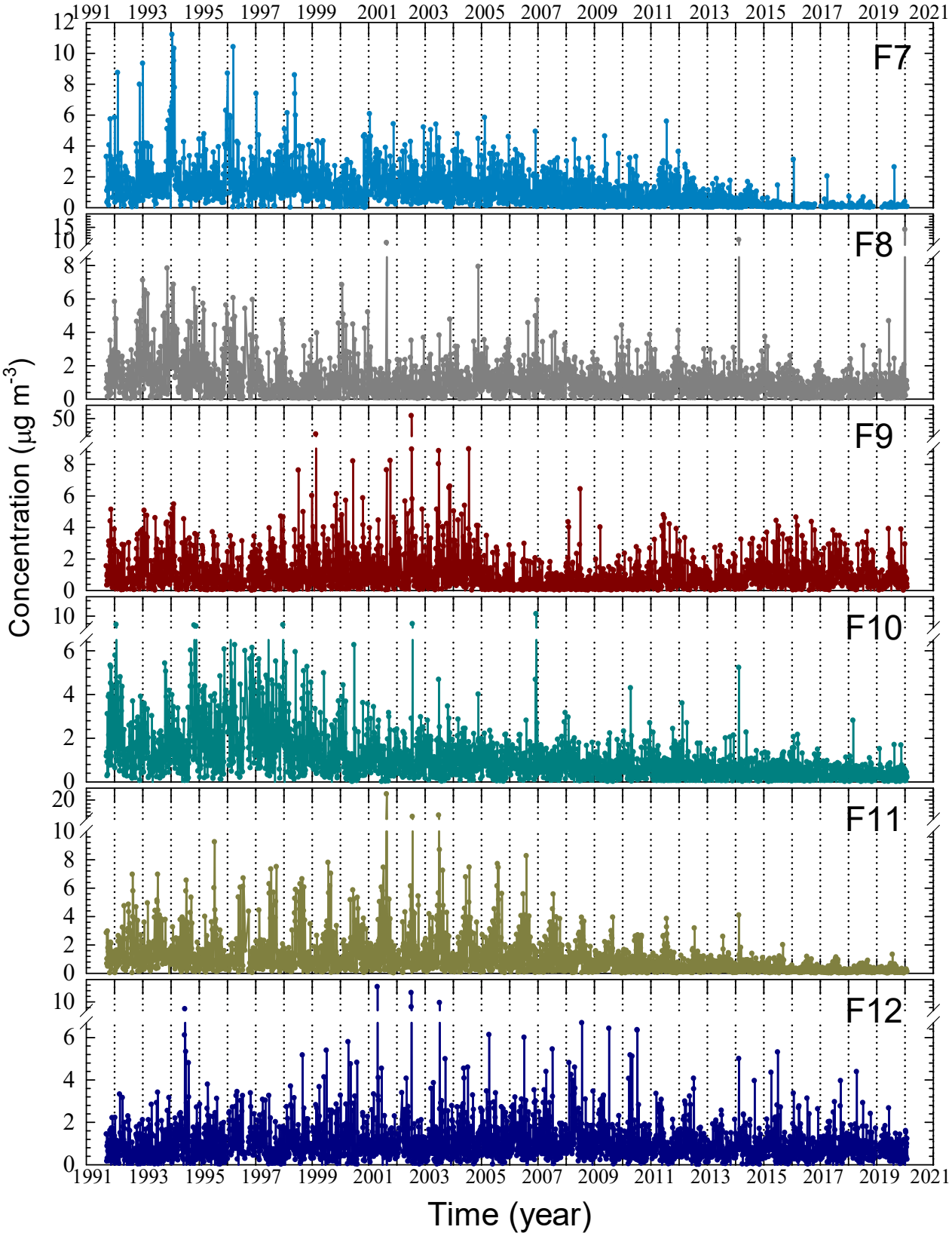

Fig. 11. Temporal variations (Mode *A*) of the factors F7-F12, obtained by the Positive Matrix Factorization (PMF) for Brigantine, New Jersey

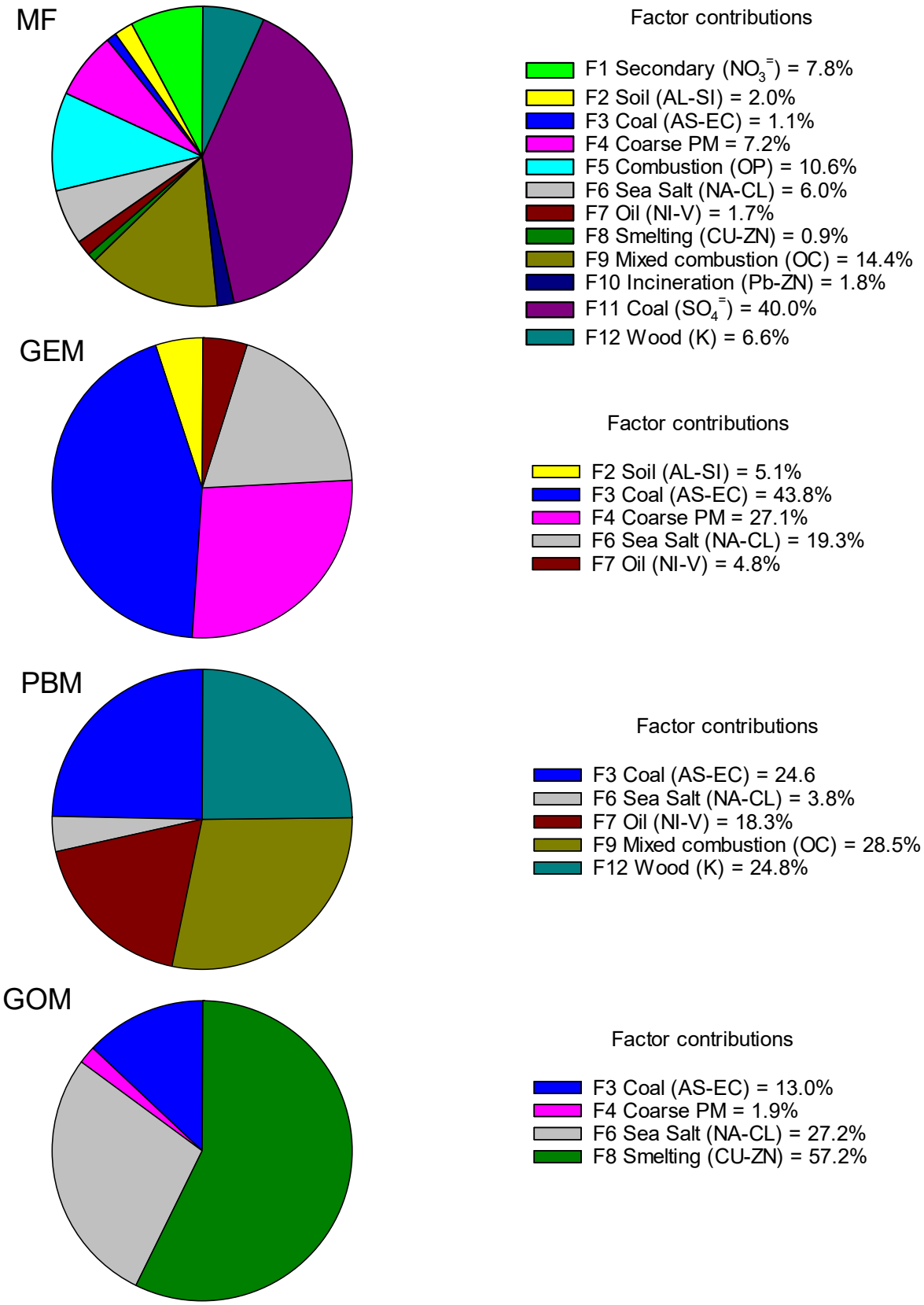

Fig. 12. Sources of $PM_{2.5}$ (MF) and mercury (GEM, PBM, and GOM), identified by the Positive Matrix Factorization for Brigantine, New Jersey

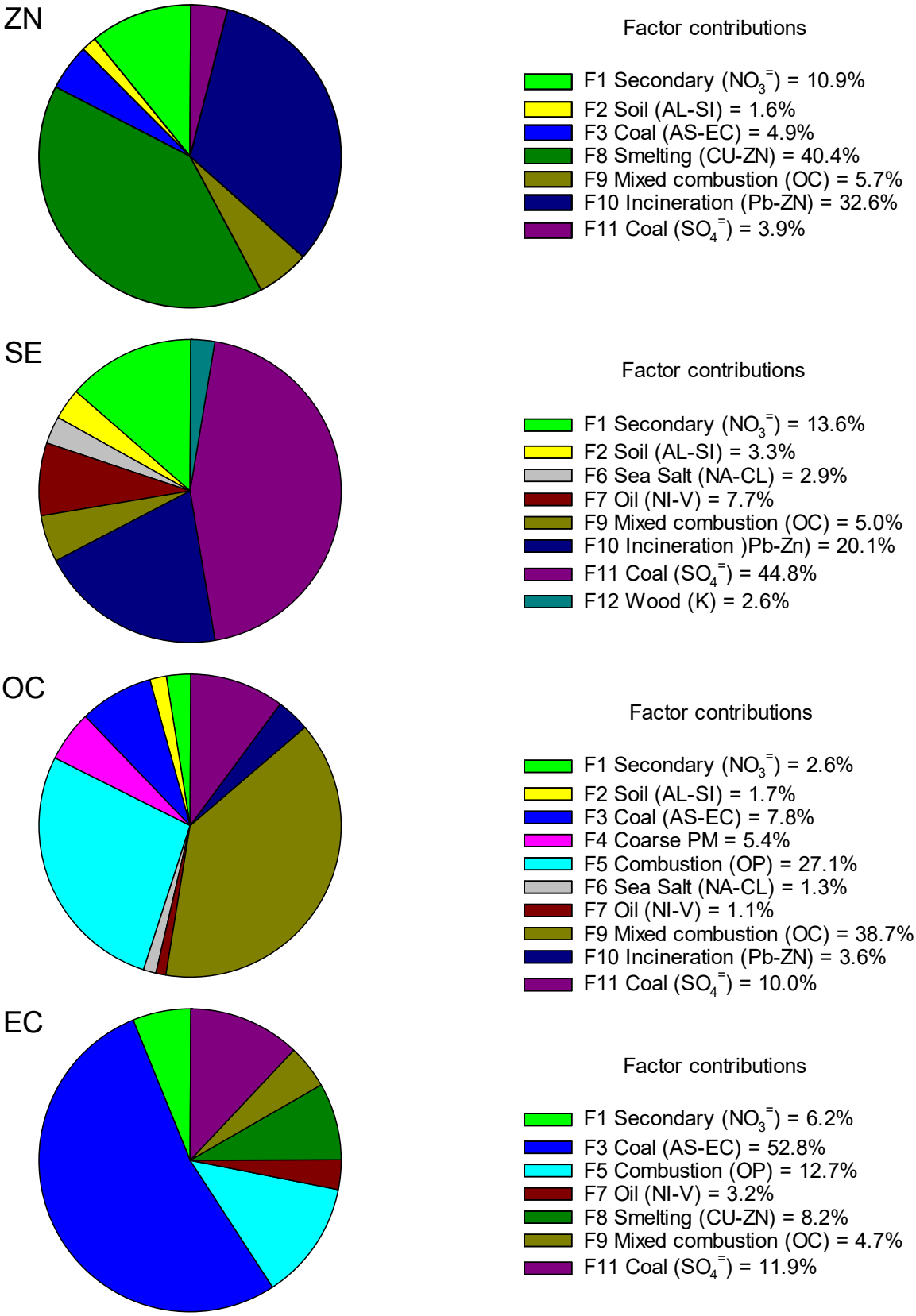

Fig. 13. Sources of zinc (ZN), selenium (SE), organic and elemental carbons (OC and EC), identified by the Positive Matrix Factorization for Brigantine, New Jersey

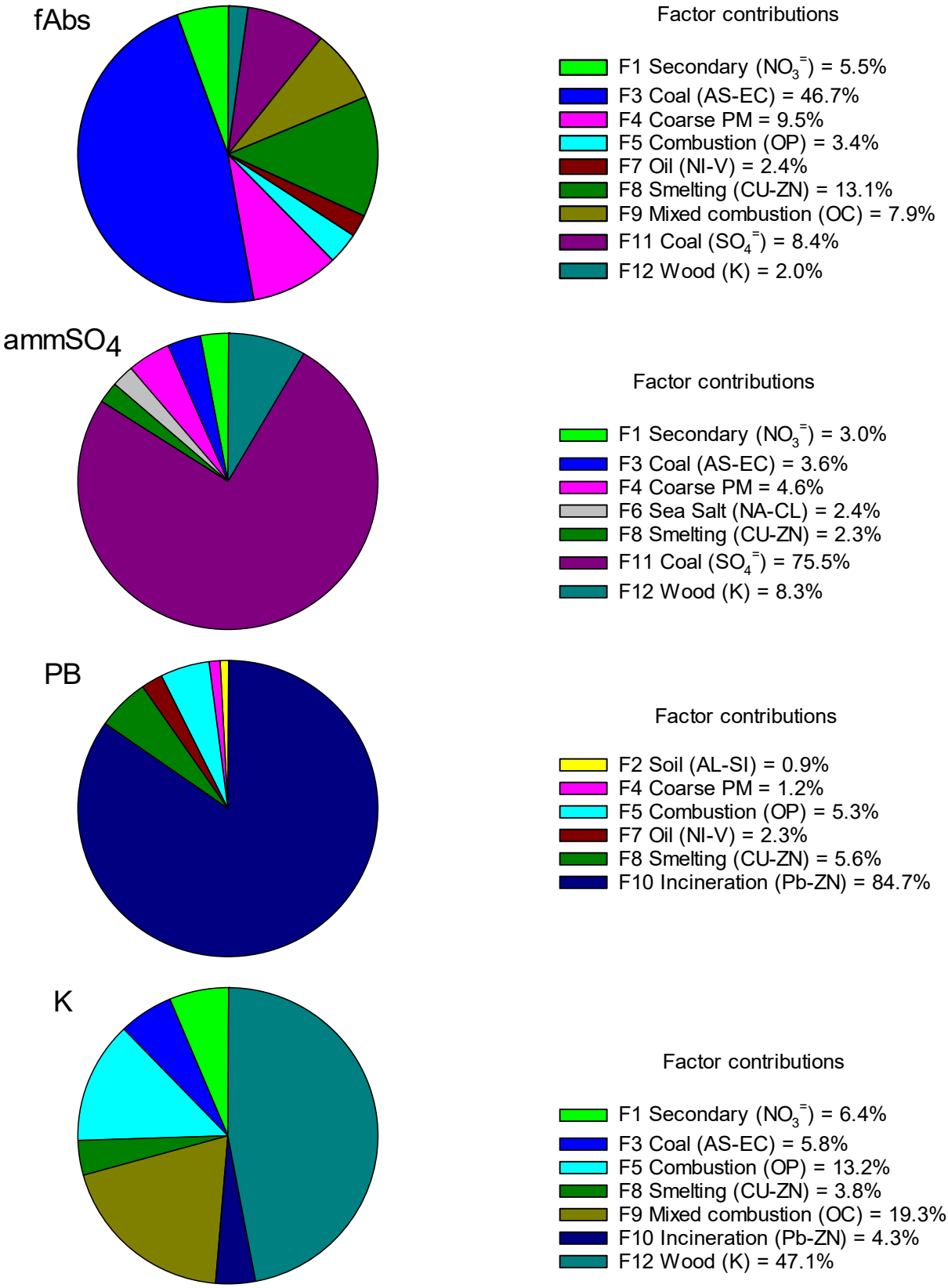

Fig. 14. Sources of absorption coefficient (fAbs), sulfate ammonium ($ammSO_4$), lead (PB), and potassium (K), identified by the Positive Matrix Factorization for Brigantine, New Jersey

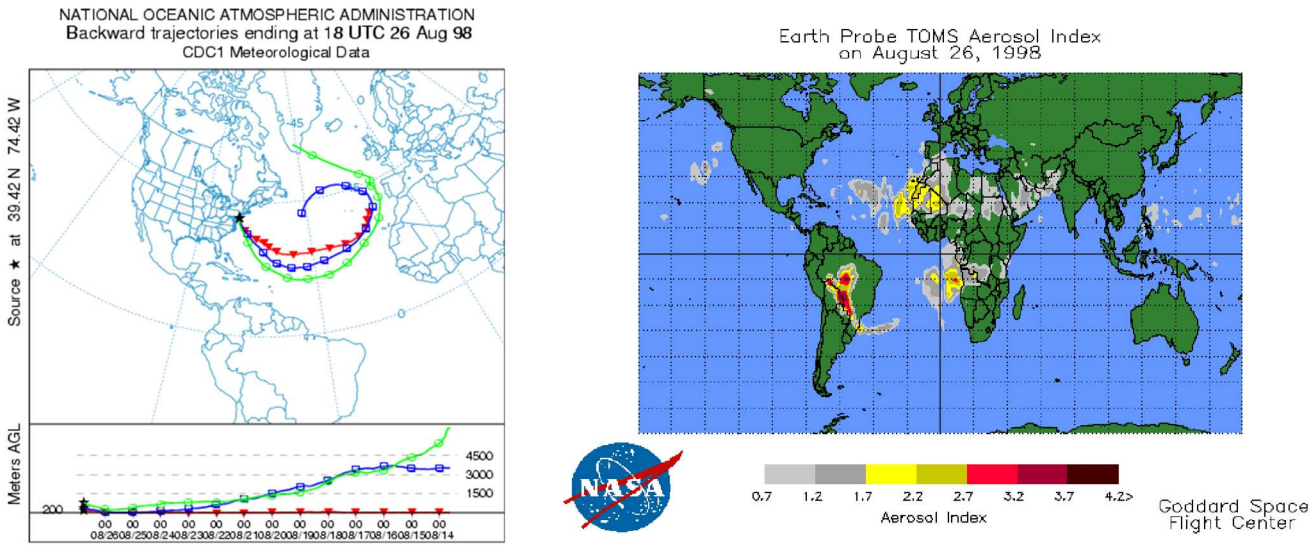

Fig. 15. An example of the backward trajectory plot and satellite picture for a day (August 26, 1998) when the soil factor F2 contribution was high (Sahara dust transport episode). The red, blue, and green lines represent backward trajectories ending at 100, 200, and 500 m elevations.

Table 2. Descriptions of the air quality parameters for the IMPROVE data set (Federal Land Manager Environmental Database, 2023) and mercury fractions, measured by NJDEP

Parameter	Code	AQSCode	Units	Description
Aluminum (Fine)	AL	88104	µg m^{-3}	Mass of aluminum particles < 2.5 µm in diameter
Ammonium Nitrate (Fine)	ammNO3	88344	µg m^{-3}	Mass of ammonium nitrate particles < 2.5 µm in diameter
Ammonium Sulfate (Fine)	ammSO4	88339	µg m^{-3}	If particulate Sulfur (Sf) is non-null, then ammSO4f is calculated as 4.125 * Sulfur. Otherwise, it is calculated as 1.375 * Sulfate (SO4f). If the concentration of the base parameter (Sf or SO4f) is below the minimum detection limit, then 0.5 * MDL is used.
Arsenic (Fine)	AS	88103	µg m^{-3}	Mass of arsenic particles < 2.5 µm in diameter
Bromine (Fine)	BR	88109	µg m^{-3}	Mass of bromine particles < 2.5 µm in diameter
Calcium (Fine)	CA	88111	µg m^{-3}	Mass of calcium particles < 2.5 µm in diameter
Chlorine (Fine)	CL	88115	µg m^{-3}	Mass of chlorine particles < 2.5 µm in diameter
Chloride (Fine)	CHL	88203	µg m^{-3}	Chloride Elemental Concentration FINE Size Fraction
Coarse Mass	CM_calc.	81103	µg m^{-3}	Calculated coarse mass = [PM_{10}] - [$PM_{2.5}$]
Chromium (Fine)	CR	88112	µg m^{-3}	Mass of chromium particles < 2.5 µm in diameter
Copper (Fine)	CU	88114	µg m^{-3}	Mass of copper particles < 2.5 µm in diameter
Carbon, Elemental Total (Fine)	EC	88307	µg m^{-3}	From TOR carbon fractions (E1+E2+E3-OP)
Carbon, Elemental Fraction 1 (Fine)	EC1	88329	µg m^{-3}	Mass of elemental carbon fraction 1 measured by TOR
Carbon, Elemental Fraction 2 (Fine)	EC2	88330	µg m^{-3}	Mass of elemental carbon fraction 2 measured by TOR
Carbon, Elemental Fraction 3 (Fine)	EC3	88331	µg m^{-3}	Mass of elemental carbon fraction 3 measured by TOR
Filter Absorption Coefficient	fAbs	63102	Mm^{-1}	A calibrated absorption coefficient measured from a Teflon filter using a hybrid integrating plate and sphere method
Filter Absorption Coefficient	fAbs_HIPS		Mm^{-1}	Absorption coefficient measured by Integrating laser integrating plate method (HIPS)
Iron (Fine)	FE	88126	µg m^{-3}	Mass of iron particles < 2.5 µm in diameter
Hydrogen	H		µg m^{-3}	Mass of hydrogen particles < 2.5 µm in diameter
Potassium (Fine)	K	88180	µg m^{-3}	Mass of potassium particles < 2.5 µm in diameter
Mass, $PM_{2.5}$ (Fine)	MF	88101	µg m^{-3}	Gravimetric mass of particles < 2.5 µm in diameter
Magnesium (Fine)	MG	88140	µg m^{-3}	Mass of magnesium particles < 2.5 µm in diameter
Manganese (Fine)	MN	88132	µg m^{-3}	Mass of manganese particles < 2.5 µm in diameter
Mass, PM_{10} (Total)	MT	85101	µg m^{-3}	Gravimetric mass < 10 um in diameter
Nitrite (Fine)	N2	88338	µg m^{-3}	Mass of nitrite particles < 2.5 µm in diameter
Sodium (Fine)	NA	88184	µg m^{-3}	Mass of sodium particles < 2.5 µm in diameter
Nickel (Fine)	NI	88136	µg m^{-3}	Mass of nickel particles < 2.5 µm in diameter
Nitrate (Fine)	NO3	88306	µg m^{-3}	Mass of nitrate particles < 2.5 µm in diameter

Carbon, Organic Total (Fine)	OC	88320	µg m^{-3}	From TOR carbon fractions (OC1+OC2+OC3+OC4+OP)
Carbon, Organic Fraction 1 (Fine)	OC1	88332	µg m^{-3}	Mass of organic carbon fraction 1 measured by TOR
Carbon, Organic Fraction 2 (Fine)	OC2	88333	µg m^{-3}	Mass of organic carbon fraction 2 measured by TOR
Carbon, Organic Fraction 3 (Fine)	OC3	88334	µg m^{-3}	Mass of organic carbon fraction 3 measured by TOR
Carbon, Organic Fraction 4 (Fine)	OC4	88335	µg m^{-3}	Mass of organic carbon fraction 4 measured by TOR
Carbon, Organic Pyrolyzed (Fine), by Reflectance	OP	88336	µg m^{-3}	Mass of pyrolyzed carbon fraction measured by TOR
Phosphorus (Fine)	P	88152	µg m^{-3}	Mass of phosphorus particles < 2.5 µm in diameter
Lead (Fine)	PB	88128	µg m^{-3}	Mass of lead particles < 2.5 µm in diameter
Rubidium (Fine)	RB	88176	µg m^{-3}	Mass of rubidium particles < 2.5 µum in diameter
Mass, $PM_{2.5}$ Reconstructed (Fine)	RCFM	88401	µg m^{-3}	Calculated fine mass = [SO4]+[NO3] +[EC]+[OC]+[SOIL]
Sulfur (Fine)	S	88169	µg m^{-3}	Mass of sulfur particles < 2.5 µm in diameter
Selenium (Fine)	SE	88154	µg m^{-3}	Mass of selenium particles < 2.5 µm in diameter
Sea Salt (Fine)	SeaSalt	88395	µg m^{-3}	1.8 x [Chloride], or 1.8 x [Chlorine] if the chloride measurement is below detection limits, missing or invalid.
Silicon (Fine)	SI	88165	µg m^{-3}	Mass of silicon particles < 2.5 µm in diameter
Sulfate (Fine)	SO4	88403	µg m^{-3}	Mass of sulfate particles < 2.5 µm in diameter
Soil (Fine)	SOIL	88348	µg m^{-3}	Calculated fine soil mass = 2.2[AL]+2.19[SI] +1.63[CA]+2.42[FE] +1.94[TI]
Strontium (Fine)	SR	88168	µg m^{-3}	Mass of strontium particles < 2.5 µm in diameter
Titanium (Fine)	TI	88161	µg m^{-3}	Mass of titanium particles < 2.5 um in diameter
Vanadium (Fine)	V	88164	µg m^{-3}	Mass of vanadium particles < 2.5 µm in diameter
Zinc (Fine)	ZN	88167	µg m^{-3}	Mass of zinc particles < 2.5 µm in diameter
Zirconium (Fine)	ZR	88185	µg m^{-3}	Mass of zirconium particles < 2.5 µm in diameter
Gaseous Elemental Mercury	Avg GEM		ng m^{-3}	Mass concentration of elemental mercury, measured by TEKRAN and averaged to correspond the IMPROVE sampling protocol
Particulate Bound Mercury	Avg PBM		ng m^{-3}	Mass concentration of particulate mercury, measured by TEKRAN and averaged to correspond the IMPROVE sampling protocol
Gaseous Oxidized Mercury	Avg GOM		ng m^{-3}	Mass concentration of oxidized mercury, measured by TEKRAN and averaged to correspond the IMPROVE sampling protocol